

GAMMA-RAY BLAZARS NEAR EQUIPARTITION AND THE ORIGIN OF THE GEV SPECTRAL BREAK IN 3C 454.3

MATTEO CERRUTI^{1,2}, CHARLES D. DERMER³, BENOÎT LOTT⁴, CATHERINE BOISSON² AND ANDREAS ZECH²

Draft version July 14, 2018

Abstract

Observations performed with the *Fermi*-LAT telescope have revealed the presence of a spectral break in the GeV spectrum of flat-spectrum radio quasars (FSRQs) and other low- and intermediate-synchrotron peaked blazars. We propose that this feature can be explained by Compton scattering of broad-line region (BLR) photons by a non-thermal population of electrons described by a log-parabolic function. We consider in particular a scenario in which the energy densities of particles, magnetic field, and soft photons in the emitting region are close to equipartition. We show that this model can satisfactorily account for the overall spectral energy distribution of the FSRQ 3C 454.3, reproducing the GeV spectral cutoff due to Klein-Nishina effects and a curving electron distribution.

Subject headings: Radiation mechanisms: nonthermal - Galaxies: active - Galaxies: individual: 3C 454.3 - gamma rays: general

1. INTRODUCTION

The Large Area Telescope (*LAT*) on board the *Fermi* Gamma ray Space Telescope (Atwood et al. 2009) has significantly improved our knowledge of the properties of active galactic nuclei (AGN) emitting GeV photons. The science of blazars, which represent more than 95% of sources in the *Fermi*-LAT extragalactic catalog (Ackermann et al. 2011), has particularly benefited thanks to *Fermi* and its all-sky observation mode. The main observational characteristics of blazars are extreme variability, a high degree of polarization, and a spectral energy distribution (SED) dominated by a non-thermal continuum at all wavelengths (see e.g. Urry & Padovani 1995). Understanding blazars therefore depends on simultaneous multiwavelength campaigns. Since the launch of the *Fermi* satellite, the γ -ray community has, for the first time, access to uninterrupted light-curves and spectral measurements of dozens of blazars in the GeV energy band.

Blazar SEDs generally exhibit two broad components. The lower-energy one is commonly ascribed to non-thermal synchrotron radiation, and peaks in a νF_ν representation between mm and X-rays, while the second one, associated in leptonic models with an inverse Compton process, peaks at γ -ray energies (see e.g. Abdo et al. 2010b). BL Lac objects show a variety of synchrotron-peak frequencies ν_{pk} , and we can thus differentiate between low-synchrotron-peaked sources (LSP, showing a peak frequency below 10^{14} Hz; see Abdo et al. 2010a), intermediate-synchrotron-peaked sources (ISP, $10^{14} \leq \nu_{pk} < 10^{15}$ Hz), and high-synchrotron-peaked (HSP) sources, with $\nu_{pk} > 10^{15}$ Hz. In contrast to BL Lac objects, FSRQs are essentially all LSP blazars.

The blazar emission arises from a relativistic jet of plasma with Doppler factor δ and magnetic field B that contains a

non-thermal population of electrons and positrons. The synchrotron emission is thought to make the low-energy component of the SED, while low-energy photons Compton-scattered to γ -ray energies make the high-energy component. The soft photons can be the synchrotron emission itself (synchrotron-self-Compton model, SSC, Konigl 1981) or an external photon field (external-inverse-Compton model, EIC), such as the emission from the BLR (Sikora et al. 1994), the dust torus (Błażejowski et al. 2000) or the accretion disk (Dermer & Schlickeiser 1993). The SSC model can satisfactorily describe the SED of HSP BL Lac objects, while for LSP blazars an external photon field is required (e.g., Ghisellini et al. 2011).

The modeling of blazars is, however, complicated by the large number of free parameters, especially for the EIC scenario. In a companion paper (Dermer et al. 2013), we have simplified the modeling by introducing equipartition relations between the energy densities of particles, photons and magnetic field, and by parameterizing the particle distribution with a log-parabolic function. While in that paper we focus on the properties of the overall SEDs produced in the equipartition scenario, and on the implications from modeling the blazar 3C 279, here we concentrate on the spectral break observed between ≈ 1 and 5 GeV in the *Fermi*-LAT spectrum of 3C 454.3 and, indeed, all LSP and ISP blazars with sufficiently good statistics (Abdo et al. 2009a,c, 2010b).

In this Letter we show that in the near-equipartition approach, a softening in the GeV spectrum is naturally produced from Klein-Nishina effects when jet electrons scatter BLR radiation, and is consistent with observations of the GeV break.

2. 3C 454.3 AND GEV SPECTRAL BREAKS

The γ -ray emission of 3C 454.3 (2251+158) at redshift $z = 0.859$, was first observed with *EGRET* (Hartman et al. 1993). Major pre-*Fermi* outbursts occurred in 2005 (Villata et al. 2006; Pian et al. 2006; Fuhrmann et al. 2006), and a large flare in 2007 was observed in γ -rays with the *AGILE* experiment (Ghisellini et al. 2007; Vercellone et al. 2008; Raiteri et al. 2008; Vercellone et al. 2009; Donnarumma et al. 2009). Since the launch of the *Fermi* mission, 3C 454.3 has been monitored in the GeV energy band, providing the first continuous long-term light-curve in γ -rays. The source ex-

¹ Harvard-Smithsonian Center for Astrophysics; 60 Garden Street, 02138 Cambridge, MA, USA.
matteo.cerruti@cfa.harvard.edu

² LUTH, Observatoire de Paris, CNRS, Université Paris Diderot; 5 Place Janssen, 92190, Meudon, France

³ Code 7653, Space Science Division, U.S. Naval Research Laboratory; 20375, Washington, DC, USA.
charles.dermer@nrl.navy.mil

⁴ CENBG, Université de Bordeaux, CNRS/IN2P3, UMR 7595, Gradignan, 33175, France

hibited several major flares in December 2009 and April 2010 (Ackermann et al. 2010), and in November 2010 (Abdo et al. 2011; Vercellone et al. 2011).

The *Fermi-LAT* observations have shown that the spectrum of this source does not follow a power-law behavior, but instead shows a clear break at an energy of a few GeV (Ackermann et al. 2010; Abdo et al. 2011). Especially interesting is that the energy of the break changes by less than a factor of two when the > 100 MeV flux changes by nearly a factor of 20. While the presence of a break is statistically significant, it is difficult to differentiate between a broken power-law model or a curved function, such as a power-law with an exponential cut-off or a γ -ray spectrum described by a log-parabolic function, over relatively short periods of time (Abdo et al. 2011). Data collected over longer month-long periods yield better statistics, but are in turn insensitive to short-term spectral variations.

Harris et al. (2012) showed that the mean spectrum of 3C 454.3 is best-fitted by a broken power-law function, even though the value of the break energy varies according to the energy range in which the fit is performed, suggesting “the presence of a curvature in the spectrum [...] as well as any break.” On the other hand, Abdo et al. (2011) showed a complex spectral behavior for the November 2010 flare, with no function clearly being preferred over the others.

3. DESCRIPTION OF THE CODE

The modeling of the SED of 3C 454.3 has been performed using a one-zone SSC model as described in Katarzyński et al. (2001), adding the computation of the EIC emission component for low-energy target photons from the BLR, the dust torus, and the accretion disk. The particle energy distribution in the emitting region is given by a log-parabolic function. The jet parameters δ , B , R , and the energy densities of the external radiation field are deduced from the equipartition relations given in Dermer et al. (2013).

3.1. EIC emission

We computed the EIC emission following the formulae described in Dermer & Menon (2009). With respect to the work presented in Dermer et al. (2013), in which we considered only the EIC emission using as a target photon field the Ly α line and the dust torus photons (with $E \cong 0.1$ eV), here we consider a more complex spectrum of emission lines. The strength of the lines, expressed as a ratio of line fluxes compared to the flux of the dominant Ly α emission line, has been fixed using the ratio-estimation provided by Telfer et al. (2002) (see Table 1). We tested other line-ratio combinations (Francis et al. 1991), which provide similar results and do not significantly modify the modeling.

We also verified the accuracy of approximating the external photon field as monochromatic for both the Ly α and the dust torus photons, as assumed in Dermer et al. (2013). Using Gaussian line profiles for the emission lines or a blackbody function for the torus emission, as used in the following calculations, does not modify significantly the results, which remain valid in the monochromatic approximation used in the companion paper. We furthermore modeled the EIC emission from the accretion-disk photons. The importance of this component depends on the distance of the blazar emitting-region from the disk. In the present treatment, we focus on a scenario where the direct accretion disk photons can be neglected, which constrains the minimum distance of the γ -ray emitting region from the central nucleus.

TABLE 1
BLR EMISSION LINES INCLUDED IN THE MODELING OF 3C 454.3

| Line | Flux | E (eV) |
|-------------------|------|--------|
| Ly α | 100 | 10.20 |
| C IV | 52.0 | 8.00 |
| Broad feature | 30.2 | 7.75 |
| Mg II | 22.3 | 4.43 |
| N V | 22.0 | 10.00 |
| O VI + Ly β | 19.1 | 12.04 |
| C III + Si III | 13.2 | 6.53 |

NOTE. — Line strengths are expressed as a ratio of the line flux to the Ly α flux, as given by Telfer et al. (2002).

3.2. Log-parabola function and equipartition relations

We consider a scenario where the particle distribution is described by a log-parabolic function, with model parameters for the energy densities of the photons, magnetic fields, and particles defined through equipartition relations. The differential electron number density $N'_e(\gamma')$ is defined through the relation

$$\gamma'^2 N'_e(\gamma') = \gamma_p'^2 N'_e(\gamma_p') \left(\frac{\gamma'}{\gamma_p'} \right)^{-b \log(\gamma'/\gamma_p')} \quad (1)$$

where γ' is the particle Lorentz factor, b is the curvature index, γ_p' is the peak Lorentz factor in the $\gamma'^2 N'_e(\gamma')$ distribution, and the primes underline the fact that all quantities are expressed in the blob comoving frame. The nonthermal electron distribution is thus characterized by three free parameters, namely b , γ_p' and $N'_e(\gamma_p')$.

The input parameters used to describe the blazar SED are (i) $L_{48} = L_{syn}/10^{48}$ erg s $^{-1}$, giving the apparent luminosity of the synchrotron component; (ii) $t_4 = t_v^{obs}/[(1+z)10^4 \text{ s}]$, giving the source variability timescale in terms of the measured variability timescale t_v^{obs} ; (iii) $\nu_{14} = (1+z)\nu_{syn}^{obs}/10^{14}$ Hz, giving the peak synchrotron frequency in the source frame in terms of the measured peak synchrotron frequency ν_{syn}^{obs} ; (iv) $\zeta_e = u'_e/u'_B$, the equipartition factor relating the nonthermal electron (u'_e) and magnetic-field (u'_B) energy densities; (v) $\zeta_s = u'_s/u'_B$, the equipartition factor relating the synchrotron (u'_s) and magnetic-field energy densities; (vi) $\zeta_{Ly\alpha} = u'_{Ly\alpha}/u'_B$, the equipartition factor relating the Ly α ($u'_{Ly\alpha}$) and magnetic-field energy densities; and (vii) b , the curvature index of the particle distribution, noted above. The presence of hadrons does not affect the spectral model, but will increase the jet power. In our calculations, we assume that the energy density of protons and ions is equal to the energy density of electrons.

These input parameters are used to deduce model parameters, namely the Doppler factor δ , the comoving fluid magnetic field B , the comoving emitting region size $R = c\delta t_v^{obs}/(1+z)$, and the principal electron Lorentz factor γ'_p , using the equations derived in Dermer et al. (2013). The normalization of the particle distribution and of the external photon field are obtained through ζ_e and ζ_* , while b is directly used as input for the code. In our calculation, we assume that the Doppler factor is related to the bulk Lorentz factor through $\delta = 2\Gamma$. This assumption is valid only if the jet is seen on-axis ($\theta_{obs} \simeq 0$). For the case of 3C 454.3, Jorstad et al. (2005) estimated θ_{obs} comprised between 0.2° and 3.9° , for different radio components. The component with the lowest value of θ_{obs} is remarkably stationary over several years with respect

TABLE 2
PARAMETERS USED FOR THE MODELLING OF 3C 454.3.

| Epoch ^a | Input | | | | | | | | Output | | | | | | |
|--------------------|----------|-------|------------|-----------|-----------|--------------------|--------------|-----|----------|------|------|-------------|-------------------|----------------|-------------|
| | L_{48} | t_4 | ν_{14} | ζ_e | ζ_s | $\zeta_{Ly\alpha}$ | ζ_{IR} | b | δ | B | R | γ'_p | $N'_e(\gamma'_p)$ | $u_{Ly\alpha}$ | L_{jet}^b |
| A | 0.7 | 10 | 0.03 | 0.6 | 0.07 | 1.3 | 1.04 | 1.0 | 22.3 | 0.76 | 6.69 | 205 | 0.15 | 1.82 | 8.6 |
| B | 2.4 | 3.5 | 0.03 | 3.5 | 0.12 | 10.5 | 8.4 | 1.0 | 39.3 | 0.56 | 4.13 | 180 | 0.56 | 2.56 | 29.1 |

^aEpochs A and B represent the low and high states of 2008 and 2010, respectively. Data and model SEDs are shown in Fig. 1.

^bTotal jet power assuming the energy density of hadrons equals that of electrons.

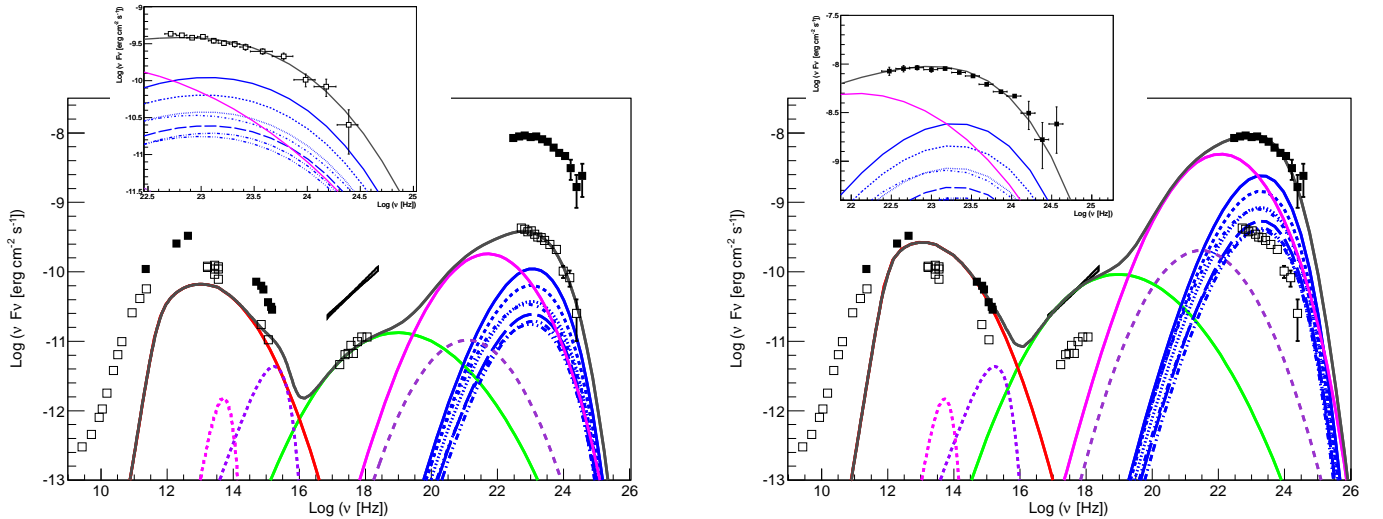


FIG. 1.— Spectral energy distribution of 3C 454.3 observed in August 2008 (open squares, see Abdo et al. 2009b) and November 2010 (full black squares, see Wehrle et al. 2012). The model components are, from low to high frequencies, the synchrotron emission (red thick line), the dust torus (magenta dotted line) and accretion disk (violet dotted line) thermal emission, the self-Compton emission (green thick line), the inverse Compton emission over the dust torus photons (magenta thick line), the inverse Compton emission over the accretion disk (violet dashed line) and the inverse Compton emission over a spectrum of emission lines, using the ratio values of Telfer et al. (2002) (blue lines, the highest one being the Ly α). The inset shows a zoom over the *Fermi-LAT* spectrum. The accretion disk and dust torus thermal emissions have been computed assuming $L_{disk} = 3.6 \cdot 10^{46}$ erg s $^{-1}$ (see Section 4), and $L_{IR} = 0.2 L_{disk}$. *Left*: modeling of the lower flux state, assuming the parameters provided in Table 2, epoch A. *Right*: modeling of the higher flux state, assuming the parameters provided in Table 2, epoch B.

to the position of the radio-core. Assuming instead a value of $\delta = \Gamma$ (corresponding to $\theta_{obs} \simeq 1/\Gamma$) does not affect the synchrotron and SSC emissions, while the normalization of the EIC components is reduced. The higher value of Γ implies as well a higher value of the jet power $L_{jet} \approx 2\pi R^2 \beta \Gamma^2 c u'_{tot}$, where u'_{tot} is the sum of all the energy densities (see, e.g., Celotti & Ghisellini 2008). However, this particular choice does not affect the modeling of the spectral break in the GeV energy range, which is the main purpose of this Letter.

4. SED MODELING

The SED of 3C 454.3 is shown in Fig. 1. Given the extreme variability observed in the γ -ray emission from this source, we have focused on two different states: a relatively low-state taken from Abdo et al. (2009b) (observations performed in August 2008, hereafter epoch A), and a high state taken from Wehrle et al. (2012) (corresponding to the highest flux state, observed in November 2010, epoch B).⁵ The UV data are modeled by the declining, high-energy part of the

synchrotron component, which peak at infrared frequencies. The blue bump emissions from the accretion disk and BLR can contribute to the UV flux measured in epoch A, while in epoch B the UV spectrum is dominated by the nonthermal continuum. The X-ray data represent, on the other hand, the rising part of the IC component, and in this scenario its origin is ascribed to the SSC component. The different EIC components produce the γ -rays observed by *Fermi-LAT*. Radio data are considered in both cases as being made by extended regions beyond the inner jet considered here, which is in accord with the lack of radiation produced at these frequencies as a consequence of synchrotron self-absorption.

The curvature parameter b of the electron distribution fits both SEDs with a value of unity. The frequency of the synchrotron peak in both epochs is assumed to be $\nu_{14} = 0.03$, though we could adjust that value if the data quality in the mm-IR regime required a different value. The variability timescale for epoch A is taken to be $t_4 = 10$, while the variability timescale for epoch B is constrained by the γ -ray variability of the flaring state and set equal to $t_4 = 3.5$, which corresponds to an observed variability timescale of roughly 18 hours (see the *Fermi-LAT* lightcurve in Wehrle et al. 2012, Fig.6). The other input parameters differ between the two

⁵ For the high-flux state, the *Fermi-LAT* data obtained during MJD 55520 have been analyzed independently from Wehrle et al. (2012). The *Fermi-LAT* data points shown in Fig. 1 come from our own analysis, giving results identical to that performed in Abdo et al. (2011).

epochs and are reported in Table 2. In particular, the synchrotron luminosity varies from $L_{48} = 0.7$ to $L_{48} = 2.4$ between epochs A and B. The ratio of the energy density of the dust to the Ly α radiation has been fixed in both cases to $\zeta_{IR}/\zeta_{Ly\alpha} = 0.8$, constrained by the low-energy *Fermi* data, and consistent with the results presented by Dermer et al. (2013) for the case of 3C 279.

As can be seen in Fig. 1, this scenario reproduces the *Fermi-LAT* observations for both the lower and the higher flux states. Note that even though the electron energy distribution is parameterized by a log-parabola function, the emission in the GeV band is not necessarily log-parabolic, given in particular the transition to the Klein-Nishina regime, and the superposition of contributions from different external photon fields (dust and lines from the BLR) with different temperatures.

Looking at the output parameters, we see that the emitting region in the high state is characterized by a larger Doppler factor (39 vs. 22) and a smaller radius (4×10^{16} cm vs. 7×10^{16} cm) and magnetic field (0.6 G vs. 0.8 G) with respect to the lower state. In order to describe the *Fermi* spectrum, the energy density of the external BLR photon field increases by roughly 40% from epoch A to epoch B.

Our modeling can be compared with the one done by Bonnoli et al. (2011). In their model, the EIC component is more important than the SSC, and contributes significantly at soft X-ray energies as well. They obtain higher magnetic field values (of the order of 4-6 G), and Doppler factors close to the value we derive for epoch A, and never higher than $\delta = 30$. The emitting region size they find is slightly smaller (10^{16} cm), but this parameter is strongly dependent on the assumed variability timescale.

The EIC scattering of the thermal photons emitted by the accretion disk depends on the assumptions made on the mass of the supermassive black hole M_{\bullet} , the Eddington luminosity ratio l_{Edd} , the accretion efficiency η , and the location of the emitting region r_{γ} . In the plots shown in Fig. 1 we have assumed $M_{\bullet} = 5 \cdot 10^8 M_{\odot}$ (Bonnoli et al. 2011), $l_{Edd} = 0.5$, $\eta = 0.1$, and $r_{\gamma} = 10^4 R_G$. In particular, if the emitting region is located closer to the accretion disk, this component becomes more important, and it starts dominating the SED when $r_{\gamma} \lesssim 3000 R_G$.

The location of the γ -ray emitting region can be constrained as well by looking at the energy densities of BLR photons (see discussion in Dermer et al. 2013). In fact, the radius of the BLR (R_{BLR}) can be inferred from the luminosity of the accretion disk, and then used to estimate the BLR photon energy density (see e.g. Ghisellini & Tavecchio 2008). For the case of 3C 454.3, following Bonnoli et al. (2011) we assumed $R_{BLR} = 6 \cdot 10^{17}$ cm ($\simeq 8 \cdot 10^3 R_G$) and $L_{disk} = 3.6 \cdot 10^{46}$ erg s $^{-1}$, which yields $u_{BLR} \simeq 0.03$ erg cm $^{-3}$. The values we derive in our modeling are two orders of magnitude lower than this estimated value, implying an emitting region located farther away, at the outer edge of the BLR, consistent with the locations deduced for the emission regions in 3C 279.

A point worth noting is the prediction of our model for the spectral behavior in the energy range between X-rays and *Fermi* where observations are lacking. In this band, EIC radiation associated with Compton-scattered torus photons dominates the flux, already indicated by Swift BAT observations (Ajello et al. 2012). The energy density of the IR radiation field, fixed in our models to 0.8 times the Ly α one, can be more tightly constrained by better hard-X-ray data. *NuSTAR* (Harrison et al. 2010) is now providing data that can help reveal this missing piece of the SED, as will *Astro-H*

(Takahashi et al. 2010).

5. DISCUSSION AND SUMMARY

The GeV spectral break in LSP and ISP blazars was not predicted, and remains one of the most interesting features in the blazar γ -ray spectrum. Various theoretical models have been developed to explain the GeV spectral break. After the original discovery of the GeV break in 3C 454.3 Abdo et al. (2009b) speculated that it was due to a break in the electron spectrum, but in this case the break energy should be strongly dependent on δ and the source flux. Finke & Dermer (2010) proposed a model in which the *Fermi-LAT* spectrum is ascribed to the superposition of an EIC emission component from target accretion-disk photons making most of the softer γ -rays in the GeV spectrum, and EIC radiation from target Ly α photons dominating the emission at energies above the break. Poutanen & Stern (2010) proposed an intriguing scenario, developed further in Stern & Poutanen (2011), where the GeV break originates from γ - γ pair-production attenuation when γ rays interact with high-ionization photons, including He Ly α photons. This requires the production of a power-law γ -ray spectrum made deep within the BLR. Harris et al. (2012) have shown, however, that the break energies are not consistent with the ones predicted by Stern & Poutanen (2011), weakening such an absorption scenario.

We have considered in detail a scenario originally suggested by Ackermann et al. (2010), where it was noticed that Klein-Nishina effects on Compton scattering of target 10.2 eV Ly α photons, the dominant BLR emission line, naturally makes a break at a few GeV, independent of δ . As shown there, a simple power-law electron distribution scattering the Ly α photons results in a spectrum too hard with respect to the spectral data. The presence of curvature in the electron distribution can remedy this difficulty.

We have applied the equipartition scenario described in a companion paper (Dermer et al. 2013), but improved by the inclusion of multiple emission lines in the BLR and use of blackbody rather than monochromatic dust spectrum, to model the SED of the well-studied FSRQ 3C 454.3. Here we have focused our attention on the origin of the break observed in the *Fermi-LAT* spectrum of this object. By introducing curvature in the particle energy distribution, and considering parameters near equipartition, we have shown that the EIC scattering of photons from the dusty torus and BLR can satisfactorily reproduce the *Fermi-LAT* data in two different flux states.

In contrast to other EIC models for this source (Bonnoli et al. 2011; Ghisellini et al. 2010), where the feature appears by choosing δ , B , and parameters describing the electron spectrum, we show that the GeV break is a natural consequence of BLR radiation scattered by electrons in a blazar jet where near-equipartition conditions hold. In this scenario, the location of the γ -ray emitting region is constrained to be $\gtrsim 10^4$ gravitational radii, where the direct accretion disk radiation makes a weak scattered flux. For 3C 454.3, like 3C 279, this indicates an emission region outside the conventional BLR, though still in an environment with significant emission-line and dust radiation.

The work of C.D.D. is supported by the Office of Naval Research and the Fermi Guest Investigator Program.

REFERENCES

- Abdo, A. A., Ackermann, M., Ajello, M., et al. 2009a, *ApJ*, 700, 597
 —. 2009b, *ApJ*, 699, 817
 —. 2009c, *ApJS*, 183, 46
 —. 2010a, *ApJ*, 715, 429
- Abdo, A. A., Ackermann, M., Agudo, I., et al. 2010b, *ApJ*, 716, 30
- Abdo, A. A., Ackermann, M., Ajello, M., et al. 2011, *ApJL*, 733, L26
- Ackermann, M., Ajello, M., Baldini, L., et al. 2010, *ApJ*, 721, 1383
- Ackermann, M., Ajello, M., Allafort, A., et al. 2011, *ApJ*, 743, 171
- Ajello, M., Shaw, M. S., Romani, R. W., et al. 2012, *ApJ*, 751, 108
- Atwood, W. B., Abdo, A. A., Ackermann, M., et al. 2009, *ApJ*, 697, 1071
- Błażejowski, M., Sikora, M., Moderski, R., & Madejski, G. M. 2000, *ApJ*, 545, 107
- Bonnoli, G., Ghisellini, G., Foschini, L., Tavecchio, F., & Ghirlanda, G. 2011, *MNRAS*, 410, 368
- Celotti, A., & Ghisellini, G. 2008, *MNRAS*, 385, 283
- Dermer, C. D., Cerruti, M., Lott, B., Boisson, C., & Zech, A. 2013, submitted to *ApJ*, arXiv 1304.6680
- Dermer, C. D., & Menon, G. 2009, High Energy Radiation from Black Holes: Gamma Rays, Cosmic Rays, and Neutrinos
- Dermer, C. D., & Schlickeiser, R. 1993, *ApJ*, 416, 458
- Donnarumma, I., Pucella, G., Vittorini, V., et al. 2009, *ApJ*, 707, 1115
- Finke, J. D., & Dermer, C. D. 2010, *ApJL*, 714, L303
- Francis, P. J., Hewett, P. C., Foltz, C. B., et al. 1991, *ApJ*, 373, 465
- Fuhrmann, L., Cucchiara, A., Marchili, N., et al. 2006, *A&AP*, 445, L1
- Ghisellini, G., Foschini, L., Tavecchio, F., & Pian, E. 2007, *MNRAS*, 382, L82
- Ghisellini, G., & Tavecchio, F. 2008, *MNRAS*, 387, 1669
- Ghisellini, G., Tavecchio, F., Foschini, L., Ghirlanda, G., Maraschi, L. & Celotti, A. 2010, *MNRAS*, 402, 497
- Ghisellini, G., Tavecchio, F., Foschini, L., & Ghirlanda, G. 2011, *MNRAS*, 414, 2674
- Harris, J. and Daniel, M. K. and Chadwick, P. M. A. 2012, *ApJ*, 761, 2
- Harrison, F. A., Boggs, S., Christensen, F., et al. 2010, in Society of Photo-Optical Instrumentation Engineers (SPIE) Conference Series, Vol. 7732, Society of Photo-Optical Instrumentation Engineers (SPIE) Conference Series
- Hartman, R. C., Bertsch, D. L., Dingus, B. L., et al. 1993, *ApJL*, 407, L41
- Jorstad, S. G., Marscher, A. P., Lister, M. L., et al. 2005, *AJ*, 130, 1418
- Katarzyński, K., Sol, H., & Kus, A. 2001, *A&AP*, 367, 809
- Konigl, A. 1981, *ApJ*, 243, 700
- Pian, E., Foschini, L., Beckmann, V., et al. 2006, *A&AP*, 449, L21
- Poutanen, J., & Stern, B. 2010, *ApJL*, 717, L118
- Raiteri, C. M., Villata, M., Chen, W. P., et al. 2008, *A&AP*, 485, L17
- Sikora, M., Begelman, M. C., & Rees, M. J. 1994, *ApJ*, 421, 153
- Stern, B. E., & Poutanen, J. 2011, *MNRAS*, 417, L11
- Takahashi, T., Mitsuda, K., Kelley, R., et al. 2010, in Society of Photo-Optical Instrumentation Engineers (SPIE) Conference Series, Vol. 7732, Society of Photo-Optical Instrumentation Engineers (SPIE) Conference Series
- Telfer, R. C., Zheng, W., Kriss, G. A., & Davidsen, A. F. 2002, *ApJ*, 565, 773
- Urry, C. M., & Padovani, P. 1995, *PASP*, 107, 803
- Vercellone, S., Chen, A. W., Giuliani, A., et al. 2008, *ApJL*, 676, L13
- Vercellone, S., Chen, A. W., Vittorini, V., et al. 2009, *ApJ*, 690, 1018
- Vercellone, S., Striani, E., Vittorini, V., et al. 2011, *ApJL*, 736, L38
- Villata, M., Raiteri, C. M., Balonek, T. J., et al. 2006, *A&AP*, 453, 817
- Wehrle, A. E., Marscher, A. P., Jorstad, S. G., et al. 2012, *ApJ*, 758, 72